



Relevance of supramolecular interactions, texture and lattice occupancy in the designer iron(II) spin crossover complexes

Anil D. Naik^a, Bernard Tinant^b, Kai Muffler^c, Juliusz A. Wolny^c, Volker Schünemann^c, Yann Garcia^{a,*}

^a Unité de Chimie des Matériaux Inorganiques et Organiques, Département de Chimie, Université Catholique de Louvain, Place L. Pasteur 1, 1348 Louvain-la-Neuve, Belgium

^b Unité de Chimie Structurale et des Mécanismes Réactionnels, Département de Chimie, Université Catholique de Louvain, Place L. Pasteur 1, 1348 Louvain-la-Neuve, Belgium

^c Technische Universität Kaiserslautern, Fachbereich Physik, Erwin-Schrödinger-Str. 56, 67663 Kaiserslautern, Germany

ARTICLE INFO

Article history:

Received 16 December 2008

Received in revised form

27 February 2009

Accepted 28 February 2009

Available online 13 March 2009

Keywords:

Spin crossover

Crystal engineering

Supramolecular chemistry

DFT

Fe^{II} mononuclear complexes

Mössbauer spectroscopy

ABSTRACT

New Fe^{II} complexes of formula [Fe(3-Br-phen)₂(NCS)₂] · Solvent (Solvent = 0.5 CH₃OH (**1**), 2 CH₂Cl₂ (**2**), desolvation of **2** (**3**), 0.5 CH₃COCH₃ (**4**) and 0 (**5**)) have been synthesized. ⁵⁷Fe Mössbauer and magnetic investigation reveal unique features atypical of classic [Fe(phen)₂(NCS)₂] polymorphs. Complex **1**, prepared by precipitation in MeOH, undergoes upon cooling below room temperature an incomplete and gradual thermally induced spin conversion, while **4** prepared by an extraction method remains mostly in the low-spin state. The non solvated compounds **3** and **5**, display a more abrupt spin crossover on cooling around $T_{1/2} = 175$ K and $T_{1/2} = 198$ K, respectively. Defects/soft lattice inclusion due to different methods of material synthesis, extent of aging, reaction medium and associated solvent molecules have enormous influence on the particle size and magnetic properties of these complexes. Scanning electron micrographs helps to establish a logical relationship among methods employed for synthesis, texture of materials and their effect on magnetic properties. The crystal structure of **2** determined in the monoclinic space group *P2/c* (100 K) reveals a mononuclear complex consisting of a distorted FeN₆ octahedron in the low-spin state, constructed from two 3-bromo-1, 10-phenanthroline and two isothiocyanato anions in *cis* position. Intermolecular interactions between mononuclear units of the S...Br, S...C(H) and π - π type afford a 2D supramolecular network. DFT calculations for the single molecule **2** reveals an energy difference between high-spin and low-spin isomers of 7 kJ/mol suggesting a slight destabilization of the low-spin state compared to [Fe(phen)₂(NCS)₂]. Normal co-ordinate analysis was also carried out for **3** and compared with experimental temperature dependent Raman spectra for **5**.

© 2009 Elsevier Inc. All rights reserved.

1. Introduction

One of the current topical research areas in solid state chemistry is the rational design of functional materials, synonymously termed crystal engineering [1]. While molecular crystal engineering explores and exploits intermolecular interactions in the frame of supramolecular chemistry [2], coordination crystal engineering deals with fabrication of microporous, low-density, crystalline solids known as metal-organic frameworks (MOFs). Major interests of such materials have been in the area of high density gas storage, fuel cell, separation and catalysis [3] which are under industrial consideration and development [4], and also recently in a juvenile but promising field of 'molecular electronics' comprising molecular magnets, opto-electronic devices, molecular switches, and smart sensors [5,6].

Miniaturisation of micro-electronics components by replacement with molecular units, designed through a 'bottom up approach', for technical applications is a challenging and intriguing subset in molecular electronics [7]. A particularly fascinating event exploited in such 'molecular units' is the spin crossover (SCO) phenomenon. In 3d⁶ Fe^{II} complexes this stems from the existence of two different electronic configurations of the metal ion. The entropy driven SCO [8] which is a reversible intra-ionic electron transfer between a diamagnetic low-spin (¹A₁) state to a thermally populated paramagnetic high-spin (⁵T₂), with technologically important properties at the crossover point, can be induced by various external stimuli such as temperature, pressure, magnetic field, or light irradiation. In the solid state, the presence of short and long range interactions can promote cooperative first order spin transitions which are of high interest. For a SCO material to be successful in this sector of nanotechnology, some decisive factors like an abrupt spin transition with hysteresis, room temperature operation, chemical stability and visible response are crucial [7,9]. The challenge here is to design strongly

* Corresponding author. Fax: +32 10 472330.

E-mail address: yann.garcia@uclouvain.be (Y. Garcia).

cooperative SCO assemblies consisting of molecular units with strong through-space interactions [9,10].

In this context, the series of Fe^{II} bis(1,10-phenanthroline) complexes, [Fe(phen)₂X₂], is a particularly suitable system to look for spin-state crossover [11]. The multiplicity of the ground state depends on the nature of the coordinated ligand in the spectrochemical series. Such series includes both HS (X = halogens, N₃, OCN, CH₃COO) and LS (X = CN, CNO, NO₂) complexes [12]. For [Fe(phen)₂(NCX)₂] (X = S, Se), Baker and Bobonich first reported the observation of an unusual change of the temperature dependence of the magnetic moment on cooling and suggested a dinuclear arrangement as a possible crystal structure [13]. Later, the SCO behaviour as well as the crystal structure of these compounds were clarified and existence of two polymorphs was established [14,15]. Now, [Fe(phen)₂(NCS)₂] is regarded as a model mononuclear SCO complex and has been extensively investigated by a wide range of physical techniques. These include magnetic susceptibility, calorimetric measurements, XPS, X-ray diffraction, X-ray absorption, ⁵⁷Fe Mössbauer, positron annihilation, muon spin relaxation [16], UV, IR, Raman, and NMR spectroscopies for exploring the effects of metal dilution, pressure, magnetic fields, light, and soft X-ray irradiation on its thermal spin transition [5c,11]. A few theoretical studies have also been performed [17,18], particularly related to assessment of the vibrational contribution to the entropy [19,20].

Several attempts to modify this phen ligand were undertaken. The nature and position of the Y substituent on the phenanthroline moiety can dramatically modify the ligand field strength for [Fe(Y-phen)₂(NCS)₂] complexes with Y = 2-Me [21], 4-R (R = Me, Cl, CN, CO₂C₂H₅ [22], CO₂C₄H₉ [23]), 5-R (R = Me, Cl, NO₂, C₆H₅ [24]) stabilising either the LS or HS state or leading to SCO with various cooperative behaviours [12,14]. However none of these compounds were characterized by X-ray diffraction and thus nothing is known on the influence of the Y substituent on the structural properties. Effect of di or poly substitution on phenanthroline are also well documented in the literature (Y = 4,7-R (R = (CH₃)₂ [25,26], Cl₂ [22,24], CO₂C₄H₉ [23], C₁₇H₃₅, 5-(OC₁₈H₃₇) [27], 5,6-(CH₃)₂ [28]; 2,9-(CH₃)₂ [28–30], 3,4,7,8-(CH₃)₄ [24], 3,5,6,8-(CH₃)₄ [24]) but the crystal structure of only one compound is known [28]. In the present work, a bromo substituent has been introduced on the 3-position of the phen ring in order to study its influence on the magnetic properties as well as on the supramolecular organization of the mononuclear complex in the crystal lattice. We report on the detailed synthesis, structural, vibrational, magnetic, theoretical and scanning electron microscopy (SEM) investigation of new Fe^{II} SCO complexes of formula [Fe(3-Br-phen)₂(NCS)₂]·nSolvent (Solvent = 0.5 CH₃OH (1), 2 CH₂Cl₂ (2), desolvated of 2 (3), 0.5 CH₃COCH₃ (4) and 0 (5)). The crystal structure of 2 in the LS state is also presented. The influence of supramolecular interactions and solvent molecules on the SCO of this system is discussed.

2. Experimental section

Materials: Commercially available reagent grade chemicals and solvents were used after appropriate purification. 1,10-phenanthroline monohydrochloride monohydrate, bromine and nitrobenzene were purchased from ACROS Organics and used as it is.

Physical measurements: ¹H and ¹³C NMR spectra were recorded at 300 MHz on a Bruker AC 300 instrument. IR spectra were recorded on a Shimadzu FTIR-84005 spectrometer using KBr discs at r.t between 4000 and 400 cm⁻¹. Raman spectra with 1064 nm excitation were recorded between 2300 to 400 cm⁻¹

with a Bruker RFS 100/s FT-Raman spectrometer (I = 200 mW) at r.t using a diode-pumped, air-cooled Nd:YAG laser as the excitation source. Temperature dependent Raman spectra were carried out using a Senterra Raman microscope over the temperature range 298–90 K. A 785 nm diode laser was used using a power of 2 mW. Diffuse reflectance spectra were recorded with a CARY 5E spectrophotometer using teflon as a reference. UV–vis spectra were recorded on a CARY 50 UV–visible spectrophotometer. Magnetic susceptibilities were measured in the temperature range of 20–300 K using a MPMS-5 SQUID magnetometer. Magnetic data were corrected for diamagnetic contributions, which were estimated from Pascal's constants. The variable temperature ⁵⁷Fe Mössbauer measurements were recorded in transmission geometry on a constant-acceleration conventional spectrometer with a 45 mCi ⁵⁷Co(Rh) source. The powder samples were sealed in aluminium foil and spectra were recorded over the temperature range 106–300 K using a liquid nitrogen cryostat. The spectra were fitted using the Recoil 1.05 Mössbauer Analysis Software [31]. Equal Debye Waller factors were assumed for the LS and HS states. The isomer shift values are given with respect to α-Fe at r.t. Thermogravimetric analyses were performed in Ar atmosphere from 298–1073 K at a heating rate of 1 K/min using a Mettler Toledo TGA/SDTA851^c coupled to a Pfeiffer ThermoStar Mass Spectrometer (TGA-MS) with an option for evolved gas analysis. Calorimetric measurements on compounds sealed in an aluminium sample holder were carried out with a Perkin-Elmer DSC-7 differential scanning calorimeter over the temperature range 298–98 K both in cooling and warming modes, with a scan rate of 5 K/min. Powder X-ray diffraction patterns were recorded on a Siemens D5000 counter diffractometer working with a Kα radiation and operating at 293 K. The samples were spread over silicon grease on the support. CHN analyses were performed at the University College London (UK). Melting point was determined with an oil bath 3937-S Buchi device. Atomic absorption analyses were carried out to estimate the percentage of iron in the samples on a Perkin-Elmer 3110 spectrometer. Samples were digested in aqueous solutions containing nitric acid (65%). Standard solutions were prepared with Mohr's salt. Scanning electron microscopy (SEM) was performed with a Gemini Digital Scanning Microscope 982 with 1 kV accelerating voltage using an aluminium sample holder.

Synthesis of the ligand: 3-Bromo-1,10-phenanthroline (3-Br-phen) was prepared following the reported method [32] from 1,10-phenanthroline monohydrochloride monohydrate and bromine in nitrobenzene. Purification by Flash column chromatography (0.6% MeOH in CH₂Cl₂) afforded a white solid in 30% yield. Further recrystallization from hot water gave white needles. The spectroscopic data were in agreement with the literature value. M.p 165 °C (164–167 °C [32]).

Synthesis of complexes: The target compounds [Fe(3-Br-phen)₂(NCS)₂]·n(Solvent) were prepared by precipitation and Soxhlet extraction [33–35]. The syntheses were carried out in freshly distilled, deoxygenated solvents, under an inert atmosphere of N₂ using Schlenk line techniques.

2.1. Precipitation method

[Fe(3-Br-phen)₂(NCS)₂]·0.5 MeOH (1). NH₄SCN (29.37 mg, 2 equiv, 0.38 mmol) in 3 mL of MeOH was mixed with a methanolic solution (3 mL) of FeCl₂·4H₂O (38.3 mg, 1 equiv, 0.19 mmol) with a pinch of ascorbic acid. The suspensions were filtered off and the clear solution was transferred by cannula technique to a warmed methanolic solution (4 mL) of 3-Br-phen (100 mg, 2 equiv, 0.38 mmol). Immediately a brownish red

precipitate was obtained, which slowly turns to bluish pink within 10–20 min of stirring. It was filtered and washed with 1 mL of cold MeOH and dried in air. Yield 102 mg (75%). Anal. Calcd for $C_{26.5}H_{16}N_6O_{0.5}Br_2S_2Fe$ (**1**) C, 45.06; H, 2.28; N, 11.98; Fe, 7.90%. Found: C, 44.90; H, 2.01; N, 11.89; Fe, 8.61%. FTIR, cm^{-1} (KBr phase): 2068w(*sh*), 2065vs, 1419s, 1101m, 916m, 836m, 721s, 471w. Slow evaporation of a dark violet dichloromethane solution of the compound gave diffraction grade crystals of $[Fe(3-Br-phen)_2(NCS)_2] \cdot 2CH_2Cl_2$ (**2**) within 10 days. These crystals readily loses solvent of crystallization in air and the desolvated crystals are of the composition $[Fe(3-Br-phen)_2(NCS)_2]$ (**3**)

2.2. Extraction method

Preparation of the precursor complex $[Fe(3-Br-phen)_3](NCS)_2 \cdot H_2O$: Ferrrous ammonium sulfate (50 mg, 1 equiv, 0.12 mmol) in 5 mL of water was added to a warmed solution of 3-Br-phen (100 mg, 3 equiv, 0.36 mmol) in 8 mL of water. The solution turned red and was stirred for 1 h. A saturated aqueous solution of NH_4SCN was added to this mixture with constant stirring. A brown precipitate was obtained immediately. After stirring for 20 min. it was filtered, washed with water and dried over P_2O_5 . Elemental analysis confirms the composition. Anal. Calcd for $C_{38}H_{23}N_8OS_2Br_3Fe$: C, 47.31; H 2.40; N 11.62; Fe 5.80%. Found: C, 47.86; H, 2.97; N, 11.98; Fe, 5.61%. Yield 101 mg (82%).

$[Fe(3-Br-phen)_2(NCS)_2] \cdot 0.5CH_3COCH_3$ (**4**). One of the 3-Br-phen molecule of $[Fe(3-Br-phen)_3](NCS)_2 \cdot H_2O$ (200 mg, 0.2 mol) was extracted continuously for a period of two weeks with acetone in a Soxhlet apparatus under nitrogen atmosphere. A pinkish compound (Yield 57 mg, 39%) obtained after solvent leaching was collected. Anal. Calcd for $C_{26}H_{14}N_6S_2Br_2Fe$: C, 45.24; H, 2.04; N, 12.26; Fe, 8.09% Found: C, 44.46; H, 1.96; N, 11.56; Fe, 8.11%. FTIR, cm^{-1} (KBr phase): 2062w(*sh*), 2059vs, 1421s, 1105m, 916m, 835m, 721s, 472w. From the leached solution, a dark violet crystalline product (Yield 51 mg, 36%), probably a rearranged complex from the leached reactants during the extraction process was isolated and based on the composition analysis it was formulated as $[Fe^{II}(3-Br-phen)_2(NCS)_2]$ (**5**). Anal. Calcd for $C_{26}H_{14}N_6S_2Br_2Fe$: C, 45.24; H, 2.04; N, 12.26; Fe, 8.09%. Found: C, 45.17; H, 2.12; N, 11.51; Fe, 8.82%. FT-IR, cm^{-1} (KBr phase): 2070w(*sh*), 2067vs, 1419s, 1101m, 916m, 838m, 721s, 476w.

X-ray crystallography: A bluish-violet single crystal of **2** with approximate dimensions $0.38 \times 0.20 \times 0.10 \text{ mm}^3$ was mounted in a nylon loop with paratone and transferred immediately in a nitrogen cold gas stream for flash cooling. The data were collected at 100K with a MAR345 image plate using $MoK\alpha$ ($\lambda = 0.71069 \text{ \AA}$) radiation. Attempts to collect data at higher temperatures failed because of crystal breakdown. The unit cell parameters were refined using all the collected spots after the integration process. The data were not corrected for absorption, but the data collection mode with high redundancy, partially takes the absorption phenomena into account. (183 images, $\Delta\phi = 3^\circ$, 21464 reflections measured for 2096 independent reflections). The structure was solved by the Patterson method followed by difference Fourier synthesis and refined by full-matrix least-squares on F^2 using SHELXL97 [36]. All the non-hydrogen atoms were refined with anisotropic temperature factors. The hydrogen atoms were calculated with AFIX and included in the refinement with a common isotropic temperature factor; they were allowed to ride on their parent atoms. Total reflections collected, 21464; independent reflections, 2096 ($R_{int} = 0.085$) of which 1806 were considered as observed ($I > 2\sigma(I)$). Data were collected up to $2\theta = 45^\circ$, completeness = 99.8%. The summary of crystallographic data and structure analysis is given in the Table 1a and b.

Table 1

(a) Crystal data and structure refinement details for **2** (b) selected bond lengths [\AA] and angles ($^\circ$) for **2**.

(a)	
Formula	$C_{26}H_{14}Br_2FeN_6S \cdot 2CH_2Cl_2$
M	860.08 g/mol
Crystal system	monoclinic
Space group	$P2/c$ (No. 13)
<i>a</i> (\AA)	10.384(4)
<i>b</i> (\AA)	10.002(4)
<i>c</i> (\AA)	16.975(7)
α ($^\circ$)	90
β ($^\circ$)	113.97(3)
γ ($^\circ$)	90
<i>V</i> (\AA^3)	1611(1)
Z	2
D_{calcd} ($g \text{ cm}^{-3}$)	1.77
<i>F</i> (000)	848
μ (mm^{-1})	3.44
Data/restraints/parameters	2096/0/198
GOF	1.061
R_1 [$I > 2\sigma(I)$], wR_2 (all data)	0.071, 0.198
$\Delta\rho$ (max/min) ($e \text{\AA}^{-3}$)	1.58/−0.91
(b)	
Fe–N(15) ^a	1.948(9)
Fe–N(15)#1	1.948(9)
Fe–N(1)#1	1.976(8)
Fe–N(1)	1.976(8)
Fe–N(4)#1	1.986(7)
Fe–N(4)	1.986(7)
N(15)–Fe–N(15)#1	93.1(4)
N(15)–Fe–N(1)#1	174.0(3)
N(15)#1–Fe–N(1)#1	87.7(3)
N(15)–Fe–N(1)	87.7(3)
N(15)#1–Fe–N(1)	174.0(3)
N(1)#1–Fe–N(1)	92.1(4)
N(15)–Fe–N(4)#1	91.7(3)
N(15)#1–Fe–N(4)#1	94.2(3)
N(1)#1–Fe–N(4)#1	82.4(3)
N(1)–Fe–N(4)#1	91.7(3)
N(15)–Fe–N(4)	94.2(3)
N(15)#1–Fe–N(4)	91.7(3)
N(1)#1–Fe–N(4)	91.7(3)
N(1)–Fe–N(4)	82.4(3)
N(4)#1–Fe–N(4)	171.5(4)
C(16)–N(15)–Fe	173.1(8)
C(14)–N(1)–Fe	130.6(6)
C(2)–N(1)–Fe	113.8(6)
C(5)–N(4)–Fe	130.2(6)
C(3)–N(4)–Fe	112.4(6)

Symmetry transformation: #1 $-x+1, y, -z+3/2$

^a Numbers in parentheses are estimated standard deviations in the least significant digits.

DFT calculations: The total energy electronic E_{el} of the isolated HS and LS isomers as well as the normal vibration modes were calculated after full geometry optimization of the respective spin state isomer. No symmetry constraints were applied for the LS isomer, the calculation for the HS isomers were done for the C_2 symmetry. All calculations were performed with the GAUSSIAN03 programme system [37]. Becke's three-parameter hybrid functional B3LYP (Becke's exchange functional [38] together with a local spin density correlation functional III [39] and a non-local correlation functional LYP [40,41]) was used for geometry optimization and the calculation of Raman and IR spectra. The split valence basis set CEP-31G [42,43] was used. To obtain the energies of the HS and LS isomers the reparametrized version B3LYP* was used [44,45] upon the optimisation with the same functional. Tight option of integration of Gaussian package was applied for all calculations. No imaginary frequencies were obtained confirming that the used geometries correspond to true energy minima.

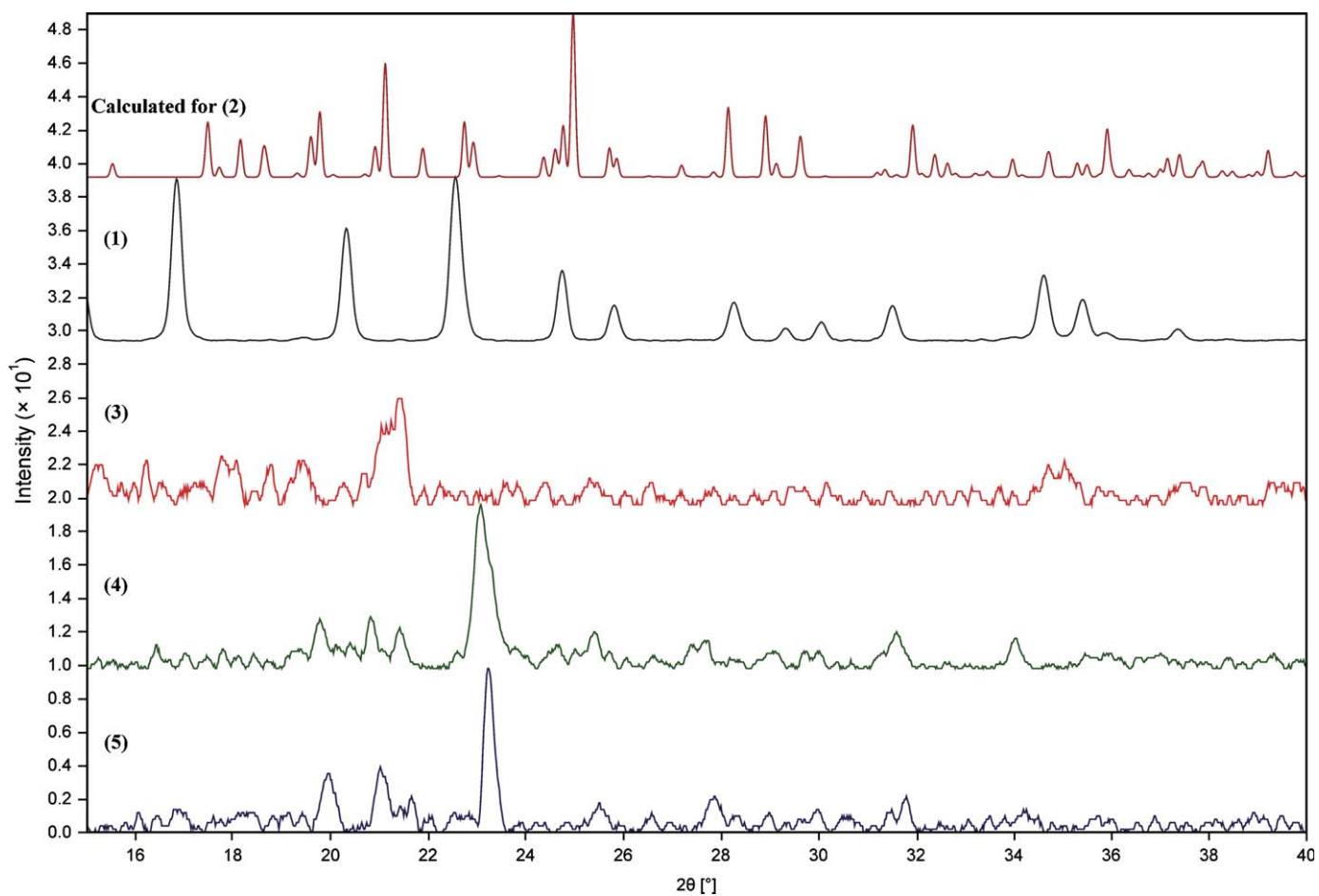


Fig. 1. X-ray powder diffractograms for **1**, **3–5** and calculated for **2** at 293 K.

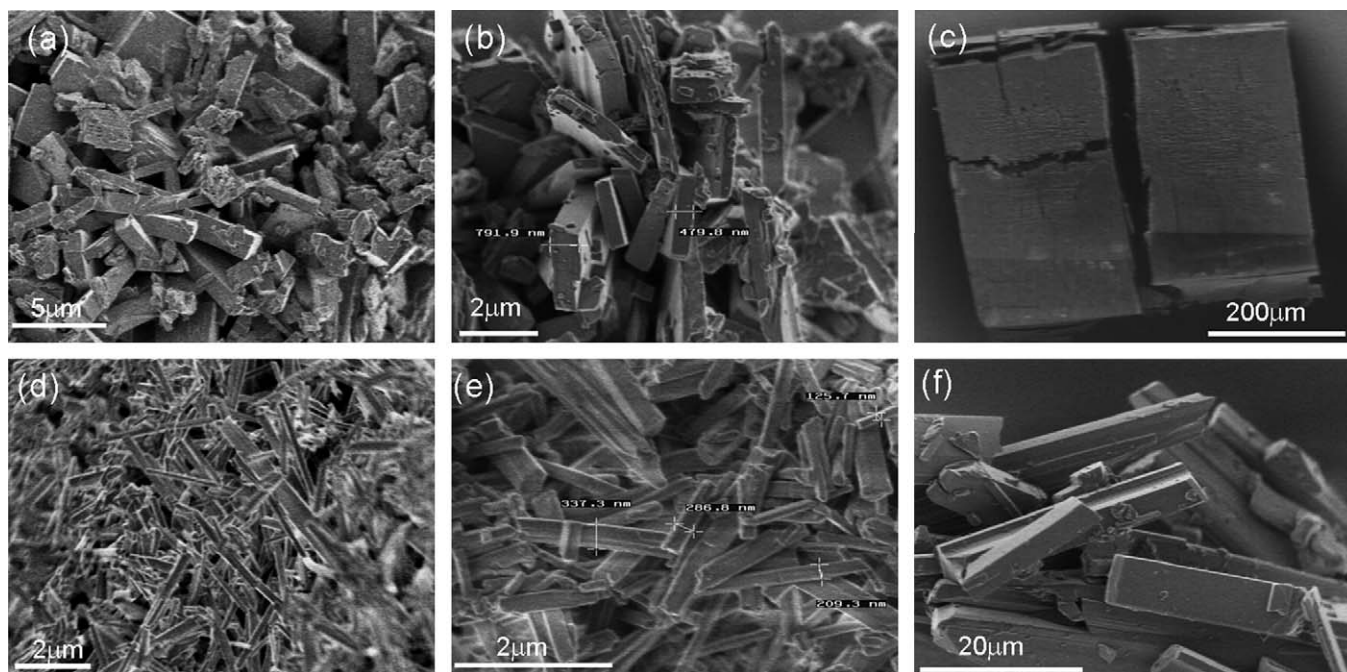


Fig. 2. SEM images of **1** (a, b), **3** (c); **4** (d, e), **5** (f).

3. Results and discussion

3.1. Synthesis

Several synthetic routes for $[\text{Fe}_2(\text{NCS})_2]$ complexes with phenanthroline based ligands *L* have been reported. The methods of preparation, workup treatment, quality of the isolated batches, solvents of preparation/crystallization have a dramatic influence on the composition and properties of the resulting complexes [33–35]. Here, we have used two preparation methods: (i) a precipitation method (ii) a Soxhlet extraction method. (i) A precipitation method in MeOH afforded immediately a brownish red precipitate which slowly turns to a bluish pink powder of formula $[\text{Fe}(\text{3-Br-phen})_2(\text{NCS})_2] \cdot 0.5\text{MeOH}$ (**1**). Rapid colour change from bluish pink to red is observed for **1** in MeOH and MeCN possibly due to isomerisation by solvolytic effect of these solvents [35]. Compound **1** is crystalline as shown by X-ray powder diffraction (Fig. 1). This feature is confirmed by SEM which reveals a mixture of microcrystals and an amorphous powder (Fig. 2a). The thickness of these crystals ranges between 450–790 nm (Fig. 2b). This crystalline character prompted us to investigate the possibility to get single crystals by recrystallization. Indeed, recrystallisation of **1** in dichloromethane afforded bluish-violet plate shaped single crystals of $[\text{Fe}(\text{3-Br-phen})_2(\text{NCS})_2] \cdot 2\text{CH}_2\text{Cl}_2$ (**2**), which were used for X-ray analysis. These crystals were highly sensitive to air and immediately break when deprived of the mother liquor due to dichloromethane release. Fig. 2c shows a SEM image of a broken crystal of **2** after exposure to air. Vertical fragmentation and lateral cracking are observed. The resulting desolvated crystals labelled as $[\text{Fe}(\text{3-Br-phen})_2(\text{NCS})_2]$ (**3**) do not have affinity for moisture, as checked by IR spectroscopy. These crystals reveal a poorly resolved X-ray powder diffractogram (Fig. 1) because of the use of small quantity of crystals. (ii) An extraction procedure in acetone afforded a pinkish powder of formula $[\text{Fe}(\text{3-Br-phen})_2(\text{NCS})_2] \cdot 0.5\text{CH}_3\text{COCH}_3$ (**4**), whose solvent composition was fixed by TGA, that reveal a fibrous character (Fig. 2d). Texture as seen by SEM imaging thus clearly indicates the effect of continuous solvent leaching method on the particles size and morphology. The parallelepiped crystals have an average thickness of 260 nm (Fig. 2e). A second compound was also obtained during the extraction procedure. Indeed, acetone leached reactants form a violet solution from which a dark violet crystalline product was isolated $[\text{Fe}(\text{3-Br-phen})_2(\text{NCS})_2]$ (**5**). SEM shows a highly crystalline character with large size crystals (2.7–6.3 μm) (Fig. 2f). Thus in the extraction method two complexes were obtained whereas only one compound was obtained for the parent complex $[\text{Fe}(\text{phen})_2(\text{NCS})_2]$.

All these compounds are soluble in CH_2Cl_2 , CHCl_3 , MeOH, EtOH, CH_3COCH_3 , MeCN, DMF and pyridine but sparingly soluble in H_2O . The formulas of all the complexes were confirmed by elemental analysis and TGA analysis.

4. Spectroscopic and thermal characterization

Study of IR, Raman, and UV–vis spectra of these complexes reveals that except subtle changes in the peak/band positions, spectra for one complex are analogous to the corresponding spectra of other complexes. IR and Raman spectra for the complexes **1** and **3–5** are depicted in Fig. 3a and assignment of experimentally observed vibrational modes for **3**, **4** and 3-Br-phen are summarized in Table S1. The thiocyanate group, which is potentially bidentate exhibits three fundamental frequencies, i.e., $\nu_1(\text{C–N stretch})$, $\nu_2(\text{N–C–S})$, and $\nu_3(\text{C–S})$, the positions of which indicate the mode of coordination [46]. The absorptions for $\nu_1 \sim 2059\text{--}2067\text{ cm}^{-1}$, $\nu_2 \sim 465\text{--}482\text{ cm}^{-1}$ and $\nu_3 \sim 835\text{--}840\text{ cm}^{-1}$

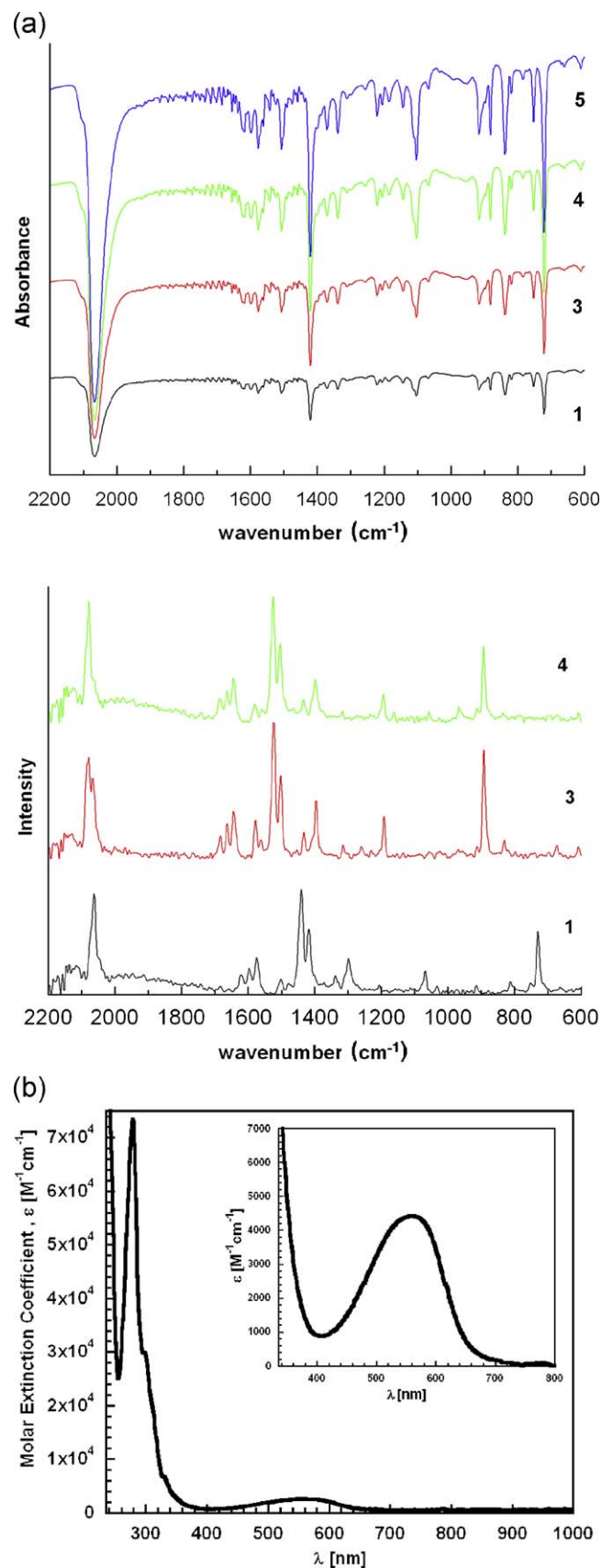


Fig. 3. (a) IR (upper, for **1**, **3–5**) and Raman (lower, for **1**, **3**, **4**) spectra recorded at 293 K. (b) Electronic spectrum of **1** in CH_2Cl_2 solution ($C = 1.14 \times 10^{-5}\text{ M}$). The inset highlights the charge transfer transition at $\lambda_{\text{max}} \approx 555\text{ nm}$ ($C = 5.6 \times 10^{-5}\text{ M}$, $\epsilon = 4411\text{ M}^{-1}\text{ cm}^{-1}$).

for all the complexes fall in the expected range of N-bonded thiocyanate. The symmetric and antisymmetric stretching vibration of the C-N band of the isothiocyanato anion observed around $2059\text{--}2067\text{ cm}^{-1}$, accompanied by a weak shoulder at higher wavenumber separated by lower than 10 cm^{-1} is taken as an indication of *cis* configuration due to stereochemical reasons. This is supported by the presence of a strong band around the same region in the Raman spectra (2062 cm^{-1}) (Table S1) [20]. This preference for *cis* arrangement is evident on the basis of molecular models, since two phenanthroline ligands cannot be accommodated in the same plane without non-bonded H-H interactions in the 2,9 position [47]. This preference is also confirmed by the crystal structure of **2** (see next section). Upon quench cooling of the sample in liquid nitrogen, no thermochromism occurs because of the dark colour of the products. Therefore no visible indication of SCO is observed. An intense visible absorption band around 555 nm (Inset to Fig. 3b), detected by UV-visible spectroscopy, in CH_2Cl_2 as shown in Fig. 3b for **1**, was assigned to a charge transfer transition while the bands observed at higher energies are essentially due to a $\pi\text{--}\pi^*$ internal ligand transition. In the region characteristic for *d-d* transitions, the room temperature diffuse reflectance spectra of all complexes do not show the multiplicity allowed band corresponding to the ${}^5T_2\text{--}{}^5E$ transition due to intense charge transfer bands tailing into the visible region.

TGA-mass spectrometry confirms the presence of solvent molecules and thermal stability of the complexes. From the thermogram shown in Fig. 4, we confirm that 0.5 solvent molecules (MeOH for **1** and acetone for **4**) are present in the samples which are presumably trapped in the voids/interstitial spaces of the crystal lattice as found for **2** (See Fig. 7). An insignificant loss of mass until 573 K is found for **5** thus confirming the absence of solvent molecules in the crystal lattice. All the complexes are remarkably thermally stable up to $\sim 580\text{ K}$, and begin to decompose above this temperature. The fact that respective solvent molecules did not escape at their boiling point during the thermogravimetric measurements indicates a strong interaction of these species with the complex molecule through supramolecular bonds [48]. Other steps in the thermogram correspond to the loss of ligands and decomposition of the complexes. The X-ray powder diffractogram (Fig. 1) of **1–5** are not similar indicating that the complexes are not isostructural. This is attributed to the different preparation methods, presence or

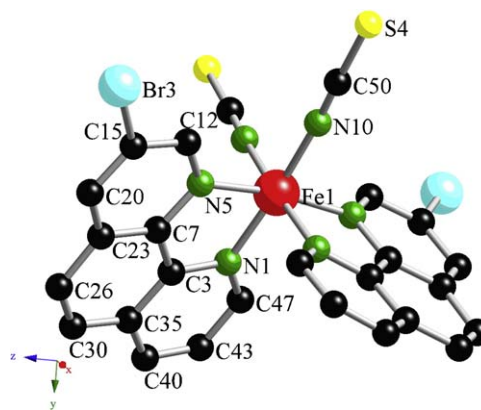


Fig. 5. Molecular structure of $[\text{Fe}(\text{3-Br-phen})_2(\text{NCS})_2] \cdot 2\text{CH}_2\text{Cl}_2$ (**2**) at 100 K . Hydrogen atoms and CH_2Cl_2 molecules are omitted for clarity.

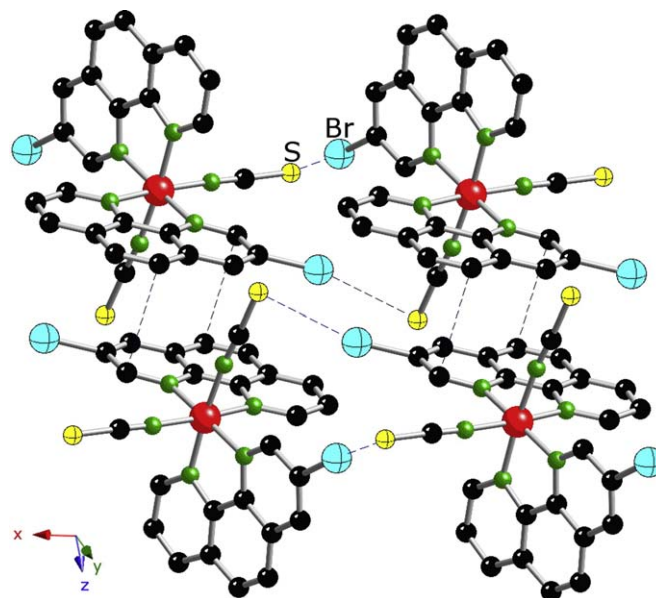


Fig. 6. Projection of the molecular structure of **2** showing $\pi\text{--}\pi$ stacking and $\text{S}\cdots\text{Br}$ interaction supporting an extended supramolecular 2D network.

absence of solvent molecules and the network reorganization induced by the loss of guest solvent molecules in the desolvated complex without modifying the structural integrity. However, compounds **4** and **5** apparently present the same structure which is due to the fact that a large time gap was taken between the synthesis and the recording of the X-ray pattern of **4**. Indeed, desolvation of acetone molecules occurred and as a result, a $\mathbf{4} \rightarrow \mathbf{5}$ transformation took place. This hypothesis was checked by TGA measurement of an aged sample of **4** ($\mathbf{4}^*$) that indicated no mass loss (Fig. 4).

5. X-ray crystallography

Complex **2** has been structurally characterized by X-ray crystallography at 100 K . Fig. 5 shows a perspective drawing of the molecule. Structural analysis revealed a monoclinic crystal system ($P2_1/c$ space group) with one half of the complex in the asymmetric part of the unit cell; the iron lying above the crystallographic two-fold axis. Two CH_2Cl_2 molecules, each one also on the two fold axis complete the structure. There are thus two CH_2Cl_2 solvent molecules per iron atom. Crystal data and refinement details for complex **2** can be found in the Table 1a.

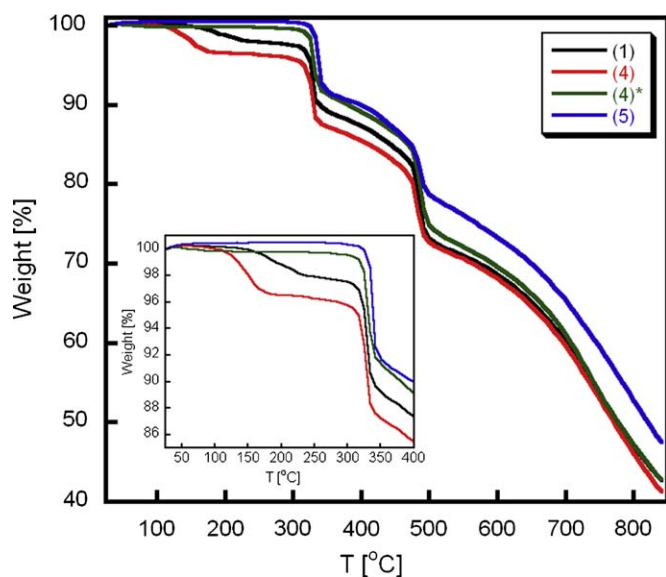


Fig. 4. Thermograms of **1**, **4**, **5** and an aged sample of **4** ($\mathbf{4}^*$).

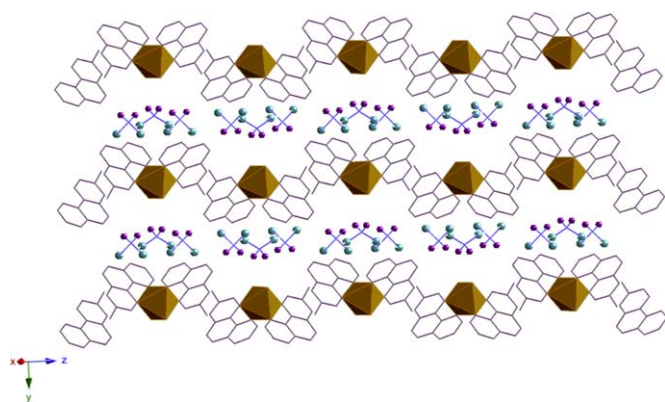


Fig. 7. Illustration of crystal packing of **2** showing trapped solvent molecules in the helical channel between the molecular units as viewed along the *a* axis.

Table 2

Observed and calculated (DFT) Raman bands for **5** in the HS and LS states. Each mode is given for both spin isomers unless differently specified for the LS one.

Raman (exp)		DFT		Mode
HS	LS	HS	LS	
298 K	90 K			
135		145	201, 204	N ^{NCS} –Fe–N ^{NCS} bending
154		175	216	N ^{NCS} –Fe–N ^{phen} bending
175	178	193	231, 237	Fe–N stretching and bending
235	366	252	330	Fe–N stretching
314	383	274	379	Fe–N stretching
			392	
334	427	332		Fe–N stretching and bending
406	489	451	429, 435, 443	SCN bending
451	530	474		Phen out-of-plane C–C–C bending
481	567	539	558	Phen out-of-plane C–C–C/in-phase bending
		560		
	673	654	672	Fe–N stretching, phen breathing
730	743	712	735	
753	754	753	741	
	792	761	759	Phen C–H in-phase out-of-plane bending
		781	770, 773	Fe–N ^{NCS} /NC–S stretching
	882	879	833, 894	Phen breathing, C–H out-of-plane bending
		881		
		899		
1066	927	1066	923	Phen C–C bending
				Phen breathing
				Fe–N stretching
	962	1104	939, 968	Phen C–H in-plane bending
				Phen C–H out of plane C–H bending
	1069	1171		Phen C–H in-plane bending
	1115	1211	1120–1173	Phen C–H in-plane bending
	1142	1234		Phen C–H in-plane bending
	1151	1244		Phen C–H in-plane bending
1204	1205	1279	1216–1244	Phen C–H in-plane bending
1300	1249	1331	1335	Phen ring stretching (Kekule)
1338	1299	1392	1439, 1449	Phen ring stretching (Kekule)
				C–H in-plane bending
1386	1338	1439	1506	Phen ring stretching
1416	1452	1447	1525	C–H in-plane bending
				Ring stretching
1440		1473	1591	Ring stretching
	1503	1507		C–H in-plane bending
1504		1519		C–H in-plane bending
1575	1565	1585		Ring stretching
1598		1603		Ring stretching
		1631		Ring stretching
		1655		
2070	2113	2046	2102	SC–N asymmetric stretching
		2063	2110	SC–N symmetric stretching

Inter-atomic distances and bond angles are listed in Table 1b. Each iron atom is octahedrally coordinated to four nitrogen atoms from two 3-Br-phen bidentate ligands and nitrogen atoms of two isothiocyanato anions in a *cis* arrangement. The Fe–N(CS) bond lengths (1.948 Å on average) are shorter than Fe–N(3-Br-phen) (1.981 Å on average). These bond lengths are typical for a LS complex. A comparison of the bond lengths and bond angles around the coordination sphere of this LS complex illustrates a distortion of the FeN₆ octahedron with a distortion parameter, $\Sigma_{LS} = 40 (2)^\circ$. The two 3-Br-phen ligands are nearly planar but orient themselves more or less perpendicular to each other around the metal ion and the maximum deviation from the best mean plane through the 14 ring atoms is 0.063(7) Å. The dihedral angle between two planes is 86(1)°. The NCS groups are nearly linear (177.4 (8)°) while Fe–N–C(S) linkages are slightly bent (173.1(8)°). The geometric constraints of the bidentate ligands cause reduction of N(3-Br-phen)–Fe–(3-Br-phen) bond angles from the ideal 90° value. The hetero aromatic planar ligand with corresponding π electrons has a potential ability to interact with the neighbouring 3-Br-phen ligand by π – π interaction [49]. Introducing bromide on the aromatic ring affords a 2D pseudo-supramolecular network constructed principally from three types of interaction around the molecule. The molecules are arranged in infinite 1D chains supported by intrachain slipped π stacking interactions between neighbouring 3-Br-phen units along *c* direction, (distance between centroids of planes N4, C3, C8, C7, C6, C5 and C2, C3, C8, C9, C10, C11 [1–*x*, –*y*, 1–*z*] = 3.759 Å, dihedral angle = 2 (1)°), a S...Br short intermolecular interaction (Fig. 6) in *a* direction (3.324(4) Å and weak intermolecular hydrogen bonding of type S...C(H) (3.675 (11) Å) in *b* direction [49]. Such S...Br–C interactions are rather uncommon [50] and have been rarely introduced in SCO complexes. The Fe...Fe separation within each chain shown in Fig. 6 is 8.49 Å which is less than between chains 10.38 Å. There are voids between the chains forming helical channels where solvent CH₂Cl₂ molecules are trapped with short contact around them (Fig. 7). Attempts to record the structure on warming was unsuccessful due to desolvation and subsequent breakdown of the crystals.

Table 3

Overview of the ⁵⁷Fe Mössbauer parameters [mm/s] for **1**, **4**, and **5**.

Entry	T [K]↑	HS			LS			A _{HS} /A _{tot}
		δ	ΔE _Q	Γ	δ	ΔE _Q	Γ	
1	143	1.19(1)	3.31(2)	0.19(1)	0.42(3)	0.32(1)	0.17(1)	0.36
	163	1.16(1)	3.17(2)	0.26(2)	0.43(1)	0.31(1)	0.19(1)	0.49
	183	1.17(1)	3.19(1)	0.19(2)	0.40(2)	0.31(3)	0.16(1)	0.51
	203	1.16(3)	3.12(2)	0.20(4)	0.37(6)	0.29(1)	0.16(1)	0.58
	223	1.15(4)	3.07(1)	0.23(1)	0.34(4)	0.27(1)	0.17(1)	0.63
	243	1.14(1)	3.02(1)	0.24(1)	0.32(4)	0.26(1)	0.18(1)	0.66
	273	1.11(2)	2.89(1)	0.21(1)	0.27(4)	0.25 ^a	0.17(1)	0.65
	293	1.09(1)	2.81(2)	0.23(1)	0.25(3)	0.3 ^a	0.20(1)	0.74
4	143	1.17(1)	3.35(2)	0.18(1)	0.38 ^a	0.32(3)	0.19(3)	0.02
	163	1.16 ^a	3.02(1)	0.18(1)	0.41(3)	0.31(1)	0.18(1)	0.10
	183	1.15(2)	3.12(1)	0.18 ^a	0.36(1)	0.30(2)	0.17(2)	0.11
	203	1.15(2)	3.13(4)	0.18 ^a	0.34(1)	0.30(6)	0.17(4)	0.12
	223	1.15(1)	3.03(4)	0.18(1)	0.32(1)	0.30(1)	0.17(2)	0.14
	243	1.15(2)	2.95(4)	0.20(3)	0.29(3)	0.30(2)	0.17(4)	0.16
	273	1.14(2)	2.81(1)	0.22(3)	0.26(4)	0.30(4)	0.18 ^a	0.16
	293	1.14(3)	2.5 ^a	0.21(1)	0.24(3)	0.30(1)	0.16(1)	0.16
5	106	1.12(1)	3.24(2)	0.2 ^a	0.23(2)	0.27(2)	0.2 ^a	0.12
	293	1.02(1)	2.62(2)	0.18(2)	0.24(2)	0.25(2)	0.2 ^a	0.5

δ: isomer shift (with respect to α-Fe at 293 K); ΔE_Q: quadrupole splitting; Γ: full width at half maximum; A_{HS}: Area of HS doublet; A_{tot}: total area.

^a Fixed parameter.

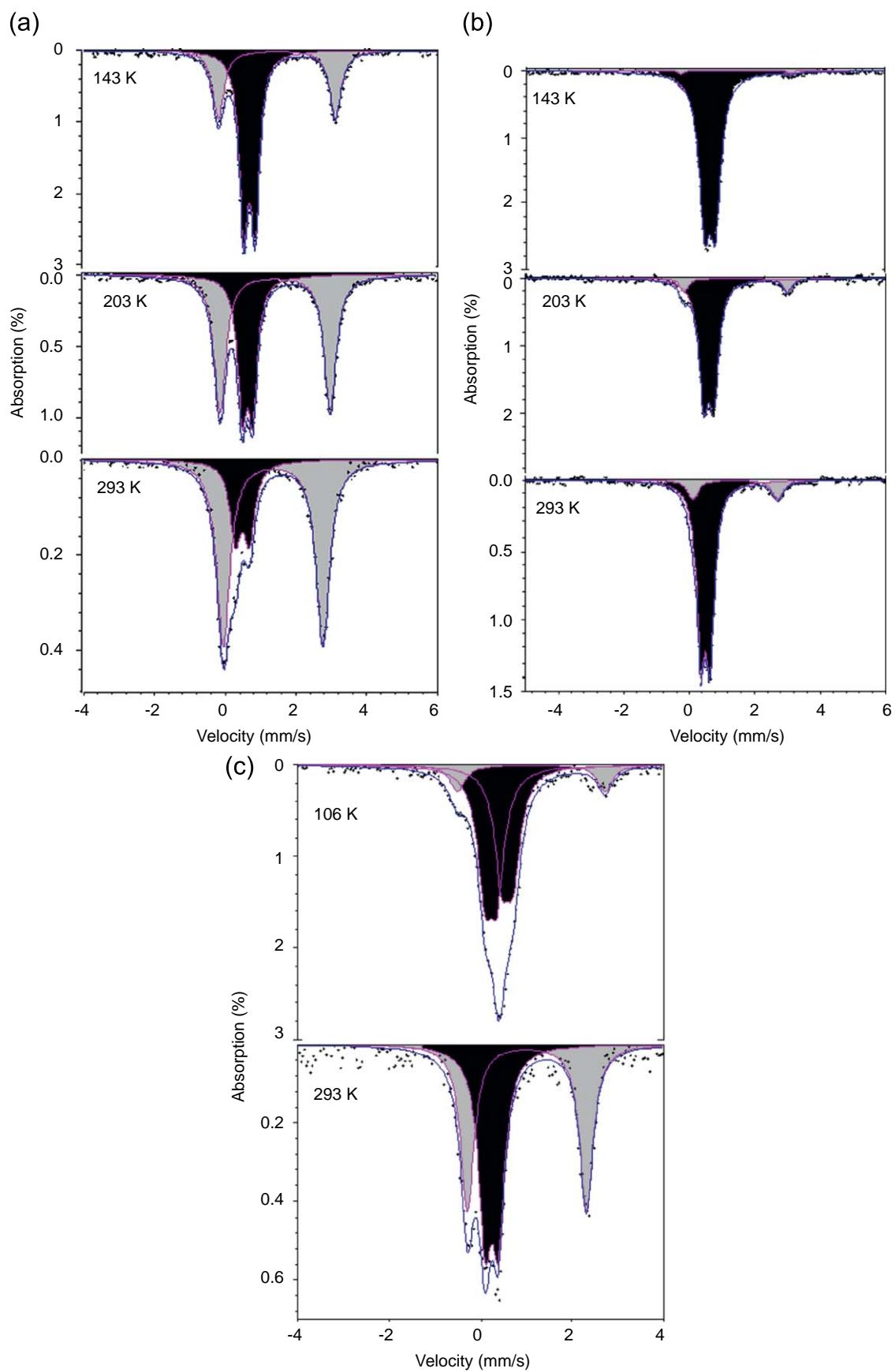


Fig. 8. Representative ^{57}Fe Mössbauer spectra of (a) **1**; (b) **4**; (c) **5** at selected temperatures. Black and grey signals correspond to the LS and HS doublets, respectively.

6. ^{57}Fe Mössbauer spectroscopy and SQUID measurements

^{57}Fe Mössbauer spectra were recorded on warming over the temperature range 106–293 K for complexes **1**, **4** and **5**. Mössbauer parameters are gathered in Table 3. Two quadrupole doublets are observed at 293 K for **1** with an isomer shift δ characteristic of the HS ($\delta^{\text{HS}} = 1.09(1)$ mm/s) and LS states ($\delta^{\text{LS}} = 0.25(3)$ mm/s) (relative to $\alpha\text{-Fe}$) (Fig. 8a). On cooling, an increase in the intensity of the LS doublet at the expense of the HS doublet is observed indicating an incomplete spin state crossover. A different behaviour is found for a fresh sample of **4** which shows a major LS signal ($\delta^{\text{LS}} = 0.24(3)$ mm/s), and a minor HS signal at 293 K whose intensity decreases on cooling thus indicating a very gradual spin conversion for a few Fe^{II} ions (Fig. 8b). The Mössbauer spectrum of **5** reveals an Fe^{II} site in equal spin state population at 293 K. On cooling to 106 K, a spin conversion to the LS state is observed, that remains however not complete because a few Fe^{II} ions are not switched. Interestingly, this spectrum had to be fitted with two LS sites at 106 K. Careful inspection of Mössbauer parameters shows an almost linear increase of isomer shifts with decrease of temperature due to second order Doppler effect [51]. More interestingly, the isomer shifts for the LS state for **1** and **4** are identical, as are those for the HS state. This indicates that there is no appreciable change in the electronic distribution around each individual iron atom. Interestingly, the local distortions revealed by the quadrupole splitting, $\Delta E_{\text{Q}}^{\text{LS}} \sim 0.3$ mm/s, is practically identical for **1**, **4** and **5**. Such a distortion for the LS octahedron was noted in the crystal structure of **2**. The HS molar fraction, γ_{HS} , assuming equal Debye–Waller factors for the LS and HS states, is plotted as a function of temperature in Fig. 9a. The spin conversion is gradual and not complete at room temperature for **1** and **4**. This gradual SCO behaviour was supported by the absence of an anomaly in the DSC measurements recorded over the temperature range 298–98 K in both cooling and warming modes for both **1** and **4**. This magnetic behaviour could stem from soft inclusions and defects that significantly decrease the propagation of spin state modifications throughout the whole lattice. In this instance, guest solvent molecules not only play a role on the spin state but also on the structural organization as shown by the dissimilar X-ray powder diffractograms among **1–5** (Fig. 1).

The magnetic properties of **3** were recorded on cooling and warming over the temperature range 20–300 K (Fig. 9b). The plot of $\chi_{\text{M}}T$ vs. T , where χ_{M} is the molar magnetic susceptibility corrected for diamagnetic contributions, shows a gradual decrease on cooling from $3.43 \text{ cm}^3 \text{ mol}^{-1} \text{ K}$ at 293 K, corresponding closely to the expected value for HS Fe^{II} centres ($S = 2$), to the lower limit of $0.46 \text{ cm}^3 \text{ mol}^{-1} \text{ K}$ at ~ 20 K corresponding to LS Fe^{II} centres ($S = 0$) with a few remaining HS Fe^{II} ions. The complex thus undergoes a gradual and incomplete spin conversion with a transition temperature $T_{1/2} = 175$ K. This more cooperative spin conversion behaviour compared to **1** and **4** suggest a framework reorganisation after solvent release where the molecular units are brought more closely in the crystal packing, thus enhancing cooperative effects. Interestingly, the transition temperature is preserved for **3** compared to $[\text{Fe}(\text{phen})_2(\text{NCS})_2]$ (polymorph I, obtained by extraction, $T_{1/2} = 177(1)$ K [10,11,13]), which is surprising since it would indicate that the bromo substitution on the phen ring has no significant effect on the spin state. This statement cannot be accounted for **5** as the SCO is shifted to a higher value ($T_{1/2} = 198$ K), thus supporting that the methods of synthesis can drastically influence the magnetic properties. Compound **5** shows indeed a gradual decrease of $\chi_{\text{M}}T$ on cooling from $2.98 \text{ cm}^3 \text{ mol}^{-1} \text{ K}$ at 300 K, corresponding to a HS state with presence of LS Fe^{II} centres ($S = 0$) to the lower limit of $0.18 \text{ cm}^3 \text{ mol}^{-1} \text{ K}$ at ~ 100 K corresponding to LS Fe^{II} centres ($S = 0$). Although, the two polymorphs **3** and **5** show similar SCO

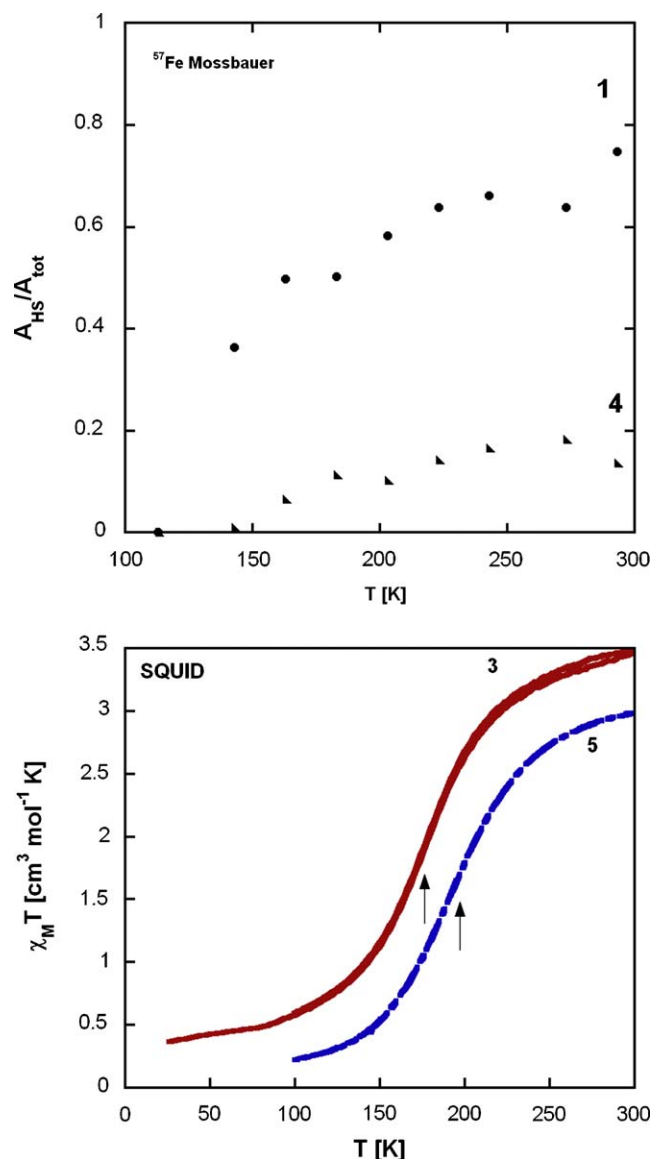


Fig. 9. (a) Temperature dependence of $A_{\text{HS}}/A_{\text{tot}}$ for **1** and **4** as deduced from ^{57}Fe Mössbauer spectroscopy (Top). (b) Thermal variation of $\chi_{\text{M}}T$ for **3** and **5** over the temperature range 20–300 K in both cooling and warming modes (Bottom). The arrow indicates the transition temperature $T_{1/2} = 175$ K for **3**; 198 K for **5**.

behaviour, the incompleteness of the transition at higher temperature differ significantly (Fig. 9b). The difference of spin state population at room temperature for **5** as deduced by the Mössbauer and the SQUID techniques (Figs. 8c and 9), though indicating an incomplete spin conversion, may stem from inequivalent Debye–Waller factors for the LS and HS states. Accurate determination of Lamb Mössbauer factors would require recording a large number data at selected temperatures for both spin states [52], which was beyond the scope of the present study.

7. DFT studies and temperature dependent Raman spectra

The computed structural parameters for $[\text{Fe}(\text{3Br-phen})_2(\text{NCS})_2]$ in the LS and HS states (B3LYP, CEP-31G) are collected in Table 4. The X-ray data for **2** as well as the X-ray data and the analogously calculated values for the parent $[\text{Fe}(\text{phen})_2(\text{NCS})_2]$ complex are given for comparison. The calculated bond lengths and angles for LS isomer are in reasonable agreement with those found by X-ray

Table 4
Principal bond lengths [Å] and bond angles [°] for the optimized structure of [Fe(3-Br-phen)₂(NCS)₂] in the HS and LS states.

Method	DFT	X-ray ^a	DFT	X-ray ^a	X-ray ^b
Spin state	HS	HS	LS	LS	LS
Fe–N _(NCS)	2.041, 2.035 ^c	2.057	1.956, 1.957, 1.946 ^c	1.958	1.948(9)
Fe–N _{(ring) trans NCS}	2.287, 2.272 ^c	2.213	1.999, 1.995 ^c	2.005	1.976(8)
Fe–N _{(ring) trans phen}	2.219, 2.201 ^c	2.199	2.015, 1.988 ^c	2.014	1.986(7)
N _(NCS) –Fe–N _(NCS)	110.9		94.0		93.1(4)
N _(ring) –Fe–N _{(ring) (cis/bite)}	75.0		82.7		91.7(3)
N _(ring) –Fe–N _{(NCS) (trans)}	160.3		174.8		173.1(8)
N _(ring) –Fe–N _{(ring) (trans)}	175.9		179.1		171.5(4)
N _(ring) –Fe–N _{(ring) (cis)}	101.9		96.7		82.4(3)
N _(ring) –Fe–N _{(NCS) (cis)}	84.1/ 90.7/ 91.6		88.4/87.2/ 92.3		91.7(3)/ 87.7(3)/94.2(3)

^a For [Fe(phen)₂(NCS)₂] [15].

^b For 2.

^c For [Fe(3-Br-phen)₂(NCS)₂].

diffraction. Interestingly enough, the obtained Fe–N distances fit even better to those determined for the parent [Fe(phen)₂(NCS)₂] particularly in the LS state [20].

The calculated multiple splitting E_S , i.e. the difference between the calculated electronic energy of HS and LS isomers (B3LYP*, CEP-31G) is 7 kJ/mol, compared to 12 kJ/mol for [Fe(phen)₂(NCS)₂] [20]. Thus, for the isolated molecule the DFT calculations predict a minor destabilisation of the LS state upon the substitution of the 3 position of phenanthroline with bromine. This situation reflects a polar (inductive) effect of the Br substituent in *meta* position. The normal co-ordinate analysis yielded all normal modes of compound **5** as well as the IR and Raman intensities. This allowed the assignment of most of IR vibrations as given in Table 2. The most intensive bands observed at room temperature at 2060, 1419 and 721 cm⁻¹, are accordingly assigned to N–CS stretching of thiocyanate, C–H in-plane bending of phen ligand and in-phase C–H out-of-plane bending of phen, respectively. DFT calculations predict these modes to give the intensive signals at 2063, 1439 and 762 cm⁻¹ for the HS isomer.

The temperature dependent Raman spectra allowed the discussion of vibrational pattern in both spin isomers. All systems reveal in an almost pure HS character at room temperature with onset of LS bands below ~243 K. The experimental results obtained for **5** combined with the DFT results are summarized in Table 2. The observed Raman vibrations for **1**, **3** and **4** are given as supplementary material (Table S2). The lines which either occur at low-temperature or significantly change their intensities upon cooling were assigned to that of the LS isomer. The comparison of room temperature and low-temperature Raman spectra for **5** is given in Fig. 10a (190 K) and in Fig. 10b (90 K). The most clear differences concern the area of 2000–2150 cm⁻¹ (SC–N stretching coupled with the Fe–N one), where a new peak due to LS isomer appears at low temperature at ca. 2100 cm⁻¹, while the splitted HS one is seen at ca. 2070 cm⁻¹. The spectral pattern is reproduced by DFT calculations which give two bands at 2102 and 2110 cm⁻¹ for LS isomer and two at 2046 and 2063 cm⁻¹ for the HS one (Fig. 10b).

The Raman spectra in 600–850 cm⁻¹ area are more difficult to interpret. With use of a 785 nm laser a strong band is observed at room temperature at ca. 735 cm⁻¹ similarly to the Raman spectra obtained with a 1064 nm laser (see Table S1), accompanied by a weaker one at 753 cm⁻¹. Upon cooling to 190 K the new bands due

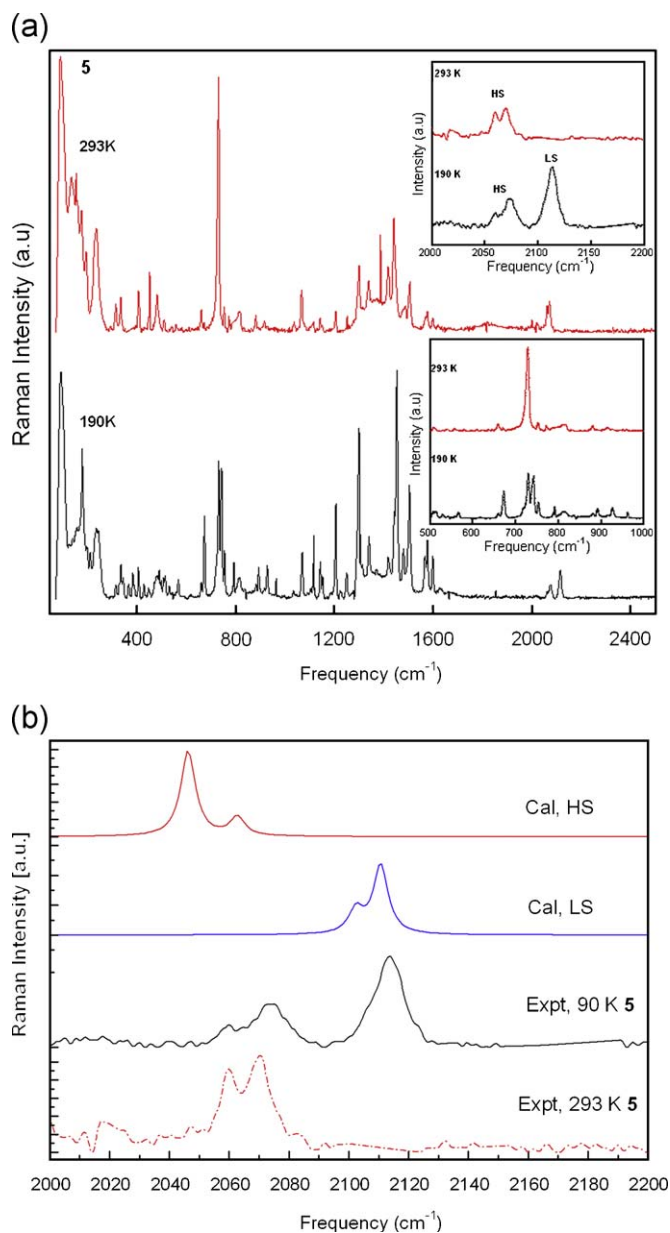


Fig. 10. (a) Raman spectra of **5** recorded at 293 K (top) and 190 K (bottom). The inset shows enlarged pictures of frequencies ranges 2000–2200 cm⁻¹ (top) and 500–1000 cm⁻¹ (bottom). (b) The observed and calculated DFT Raman spectra of **5** in the 2000–2220 cm⁻¹ region. Red and blue lines depict the calculated Raman spectra of HS and LS isomers, respectively. The red and green dashed lines are the experimental spectra measured at 293 K and 90 K, respectively. (For interpretation of the references to colour in this figure, the reader is referred to the web version of the article.)

to LS isomer appear at 673, 743 and 792 cm⁻¹. For the parent [Fe(phen)₂(NCS)₂] the bands in 765–775 cm⁻¹ were previously interpreted to be due to NC–S stretching [20] in both spin isomers. Our calculations predict these vibrations to occur at 770–780 cm⁻¹ with no significant difference between LS and HS state. On the other hand, the foregoing DFT results (see Table 2) predict few vibrations in the 650–750 cm⁻¹ region being due to phenanthroline ring stretching and the coupled Fe–N stretching, as well as C–H out-of-plane bending at 760 cm⁻¹. Thus an unambiguous assignment of the bands in this region is rather difficult.

Overall, there are no significant differences of the vibrational pattern between the title system and the parent [Fe(phen)₂

Table 5
Survey of key structural and magnetic data among members of [Fe(L)₂(NCS)₂] complexes of the 1, 10 phenanthroline (phen) family.

Complexes	Space group	Fe–N(CS)	Fe–N(L)	T _{1/2} (K)	Spin state	Σ (°)	Interactions	Reference
[Fe(bipy) ₂ (NCS) ₂]	<i>Pcbn</i> 110 K	1.945(3)	1.966(3)	213	LS	45	S...C; π–π	[61]
[Fe(phen) ₂ (NCS) ₂] Polymorph II	<i>Pcbn</i> 130 K	1.958(4)	2.009(4)	176	LS	35	S...C; π–π	[15]
[Fe(bt _z) ₂ (NCS) ₂]	<i>Pcbn</i> 130 K	1.948(8)	1.973(7)	225	LS	47	S...C; S...S; π–π	[62]
[Fe(3-Br-phen) ₂ (NCS) ₂] · 2CH ₂ Cl ₂	<i>P2/c</i> 100 K	1.948(9)	1.980	175	LS	40	S...C; S...Br; S...S; π–π,	This work
[Fe(dpp) ₂ (NCS) ₂] · py	<i>Pn</i> 293 K	2.10	2.20	163 ↑, 123 ↓	HS	76	S...C; S...S; π–π	[49]

L = respective ligand; bipy = 2,2'-bipyridine; btz = 2,2'-bi-4,5-dihydrothiazine, dpp = dipyrido[3,2-a:2'3'-c]phenazine.

Σ = sum of deviation of each of the 12 *cis* angles from 90°.

↑ or ↓ refer to heating or cooling modes, respectively.

(NCS)₂], also with respect to frequencies of the NCS fragments involved in a network of interactions with Br atoms as seen by single crystal X-ray diffraction.

8. Conclusions

The brief comparison of the magnetic properties of polymorphs I and II of [Fe(phen)₂(NCS)₂] [10] with those of our complexes reveals that the incomplete but abrupt SCO behaviour in polymorph II of the parent system (obtained by precipitation) can not be comparable with that of complex **1** due to the presence of MeOH molecules in the crystal lattice, that can dramatically influence the spin state [5]. Similarly, the complete and abrupt SCO in polymorph I (obtained by extraction) should be better compared to the non solvated compound **5** rather than compound **4** which is solvated. Nevertheless, solvent removal is beneficial for this system since it results in a more abrupt SCO behaviour and a better transmission of elastic cooperative effects (**3**, **5** compared to **1**, **4**). Interestingly, these compounds are made of larger particles than the ones presenting a smoother spin conversion (i.e. **1**, **4**) as shown by SEM imaging. Thus, reducing particle size results in reducing cooperative effects as predicted by a recent theoretical model for SCO nanoparticles [53] and noted for [Fe(pz)Pt(CN)₄] (pz = pyrazine) [54]. This result is particularly attractive in the frame of the current miniaturization of SCO molecular units at the nanometer scale [54–58] in view of their potential use in information storage devices thanks to micro and nanopatterning [59,60].

From a crystal engineering point of view, the introduction of a bromine onto the periphery of the phen ring strengthens intermolecular interactions between complex molecules affording a 2D supramolecular network. Indeed, in addition to S...C–C (3.675(11) Å) and π–π stacking interactions also present in [Fe(phen)₂(NCS)₂] [10], S...Br–C = 3.324(4) Å interactions are added for **2** for the first time in this system. The strength and directionality of such intermolecular interactions is essential to observe a cooperative spin transition. Indeed, in the case of [Fe(dpp)₂(NCS)₂] · py (dpp = dipyrido[3,2-a:2'3'-c]phenazine) [49] that present strong π–π stacking and van der Waals interactions (Table 5), a fairly abrupt spin transition with a thermal hysteresis of 40 K was observed contrary to [Fe(3-Br-phen)₂(NCS)₂] · nSolvent.

The DFT calculations for the isolated molecule reveal that the energy difference between the spin isomers is slightly less (ca. 5 kJ/mol) than that for the parent compound [Fe(phen)₂(NCS)₂] (T_{1/2} = 175 K, polymorphs I and II), suggesting a slight destabilization of the LS isomer by means of polar effect of bromine.

However, the transitions temperatures for polymorphs [Fe(3-Br-phen)₂(NCS)₂] appear to be identical or slightly higher {T_{1/2} = 175 K (**3**) and 198 K (**5**)}. Such differences that cannot be yet taken into account by computations on single molecules result from intermolecular Fe–NCS...Br interactions that directly influence the electronic density at the ligand site and thus the spin state.

Supplementary material

CCDC 687148 for **2** contains the supplementary crystallographic data for this paper. These data can be obtained free of charge from the Cambridge Crystallographic Data Center via www.ccdc.cam.ac.uk/data_request/cif.

Acknowledgements

We acknowledge financial support from FSR-UCL, IAP-VI (P6/17) INANOMAT, FNRS (FRFC and Crédit au Chercheur). KM, JAW and VS acknowledge the financial support by the BMBF (05-KS7UK2) and the DFG (Schu 1251/9-1). We thank Dr. R. Lapouyade (CNRS, Bordeaux) for providing initial sample of 3-Br-phen, Dr. V. Mishra and Prof. F. Varret for SQUID measurements as well as N. Deligne for SEM measurements.

Appendix A. Supplementary material

Supplementary data associated with this article can be found in the online version at 10.1016/j.jssc.2009.02.035.

References

- [1] G.R. Desiraju, *Crystal Engineering*, Elsevier, Amsterdam, 1989.
- [2] [a] J.M. Lehn, *Supramolecular Chemistry: Concepts and Perspectives*, VCH, Weinheim, 1995;
[b] G. Desiraju, *Angew. Chem. Int. Ed.* 46 (2007) 8342.
- [3] [a] S. Kitagawa, R. Kitaura, S. Noro, *Angew. Chem. Int. Ed.* 43 (2004) 2334–2375;
[b] S. Kitagawa, K. Uemura, *Chem. Soc. Rev.* 34 (2005) 109.
- [4] N.L. Rosi, J. Eckert, M. Eddaoudi, D.T. Vodak, J. Kim, M. O'Keeffe, O.M. Yaghi, *Science* 300 (2003) 1127–1129.
- [5] [a] P. Gütllich, A. Hauser, H. Spiering, *Angew. Chem.* 106 (1994) 2109–2141;
P. Gütllich, A. Hauser, H. Spiering, *Angew. Chem., Int. Ed. Engl.* 33 (1994) 2024–2054;
[b] P. Gütllich, Y. Garcia, H.A. Goodwin, *Chem. Soc. Rev.* 29 (2000) 419–427;
[c] P. Gütllich, Y. Garcia, H. Spiering, in: J.S. Miller, M. Drillon (Eds.), *Magnetism: From Molecules to Materials*, vol. IV, Wiley-VCH, Verlag GmbH, 2003, p. 271.

- [6] P. Gütllich, H.A. Goodwin (Eds.), *Spin Crossover in Transition Metal Compounds*. Topics in Current Chemistry, Springer, Berlin-Heidelberg, 2004, pp. 233–235.
- [7] [a] O. Kahn, J. Kröber, C. Jay, *Adv. Mater.* 4 (1992) 718–728;
[b] O. Kahn, C.J. Martinez, *Science* 279 (1998) 44–48.
- [8] M. Sorai, S. Seki, *J. Phys. Chem. Solids* 35 (1974) 555–570.
- [9] [a] Y. Garcia, V. Ksenofontov, P. Gütllich, *Hyperfine Interactions* 139/140 (2002) 543–551;
[b] Y. Garcia, V. Niel, M.C. Muñoz, J.A. Real, *Top. Curr. Chem* 233 (2004) 229–259.
- [10] [a] J.A. Real, A.B. Gaspar, V. Niel, M.C. Muñoz, *Coord. Chem. Rev.* 236 (2003) 121–141;
[b] J.A. Real, A.B. Gaspar, M.C. Muñoz, *Dalton Trans.* 12 (2005) 2062–2079.
- [11] P. Gütllich, *Struct. Bonding* 44 (1981) 83–195.
- [12] M.A. Halcrow, *Polyhedron* 26 (2007) 3523–3576.
- [13] W.A. Baker, H.M. Bobonich, *Inorg. Chem.* 3 (1964) 1184–1188.
- [14] E. König, K. Madeja, *Inorg. Chem.* 6 (1967) 48–55.
- [15] B. Gallois, J.A. Real, C. Hauw, J. Zarembowitch, *Inorg. Chem.* 29 (1990) 1152–1158.
- [16] Y. Garcia, V. Ksenofontov, S.J. Campbell, J.S. Lord, Y. Boland, P. Gütllich, *J. Phys. Chem. B* 108 (2004) 17838–17844.
- [17] M. Reiher, *Inorg. Chem.* 41 (2002) 6928–6935.
- [18] H. Paulsen, L. Duelund, H. Winkler, H. Toftlund, A.X. Trautwein, *Inorg. Chem.* 40 (2001) 2201–2203.
- [19] G. Brehm, M. Reiher, S. Schneider, *J. Phys. Chem. A* 106 (2002) 12024–12034.
- [20] K.L. Ronayne, H. Paulsen, A. Hofer, A.C. Dennis, J.A. Wolny, A.I. Chumakoy, V. Schunemann, H. Winkler, H. Spiering, A. Bousseksou, P. Gutlich, A.X. Trautwein, J.J. McGarvey, *Phys. Chem. Chem. Phys.* 8 (2006) 4685–4693.
- [21] E. König, G. Ritter, K. Madeja, A. Rosenkranz, *J. Inorg. Nucl. Chem.* 34 (1972) 2877–2886.
- [22] E. König, G. Ritter, W. Irlner, B. Kanellakopoulos, *J. Phys. C* 10 (1977) 603–615.
- [23] K. Madeja, W.H. Boehmer, N.T. Thuy; G. Oehme, A.A. El-Saghier, A. Vertes, K. Burger, *Z. Anorg. Allg. Chem.* 447 (1978) 5–17.
- [24] A.J. Cunningham, H.K. Powell, E. Sinn, H. Wong, *J. Chem. Soc. Dalton Trans.* (1972) 2155–2160.
- [25] E. König, G. Ritter, B. Kanellakopoulos, *J. Phys. C* 7 (1974) 2681–2690.
- [26] E. König, G. Ritter, S.K. Kulshreshtha, C. Csataru, *Inorg. Chem.* 23 (1984) 1903–1910.
- [27] [a] A. Ruaudel-Texier, A. Barraud, P. Coronel, O. Kahn, *Thin Solid Films* 160 (1988) 107–115;
[b] P. Coronel, A. Barraud, R. Claude, O. Kahn, A. Ruaudel-Texier, J. Zarembowitch, *J. Chem. Soc. Chem. Commun.* (1989) 193–194.
- [28] D.C. Figg, R.H. Herber, J.A. Potenza, *Inorg. Chem.* 31 (1992) 2111–2117.
- [29] B.W. Dockum, W.M. Reiff, *Inorg. Chim. Acta* 35 (1979) 285–287.
- [30] E. König, G. Ritter, K. Madeja, *J. Inorg. Nucl. Chem.* 43 (1981) 2273–2280.
- [31] K. Lagarec, D.G. Rancourt, Recoil, *Mössbauer Spectral Analysis Software for Windows 1.0*, Department of Physics, University of Ottawa, Canada, 1998.
- [32] D. Tzalis, Y. Tor, S. Failla, J.S. Siegel, *Tetrahedron Lett.* 20 (1995) 3489–3490.
- [33] P. Ganguli, P. Gütllich, E.W. Müller, *J. Chem. Soc., Dalton Trans.* (1981) 441–446.
- [34] R. Herber, M. Casson, *Inorg. Chem.* 25 (1986) 847–852.
- [35] [a] S. Savage, Z. J-Long, A.G. Maddock, *J. Chem. Soc. Dalton Trans.* (1985) 991–996;
[b] K.J. Lee, I. Yoon, S.S. Lee, B.Y. Lee, *Bull. Korean Chem. Soc.* 23 (2002) 399–403.
- [36] [a] G.M. Sheldrick, *SHELX97: Program for Crystal Structure Refinement*, University of Göttingen, Germany, 1997;
[b] A.L. Spek, *PLATON, A Multipurpose Crystallographic Tool*, University of Utrecht, The Netherlands, 1998.
- [37] M.J. Frisch, G.W. Trucks, H.B. Schlegel, G.E. Scuseria, M.A. Robb, J.R. Cheeseman, J.A. Montgomery Jr., T. Vreven, K.N. Kudin, J.C. Burant, J.M. Millam, S.S. Iyengar, J. Tomasi, V. Barone, B. Mennucci, M. Cossi, G. Scalmani, N. Rega, G.A. Petersson, H. Nakatsuji, M. Hada, M. Ehara, K. Toyota, R. Fukuda, J. Hasegawa, M. Ishida, T. Nakajima, Y. Honda, O. Kitao, H. Nakai, M. Klene, X. Li, J.E. Knox, H.P. Hratchian, J.B. Cross, C. Adamo, J. Jaramillo, R. Gomperts, R.E. Stratmann, O. Yazyev, A.J. Austin, R. Cammi, C. Pomelli, J.W. Ochterski, P.Y. Ayala, K. Morokuma, G.A. Voth, P. Salvador, J.J. Dannenberg, V.G. Zakrzewski, S. Dapprich, A.D. Daniels, M.C. Strain, O. Farkas, D.K. Malick, A.D. Rabuck, K. Raghavachari, J.B. Foresman, J.V. Ortiz, Q. Cui, A.G. Baboul, S. Clifford, J. Cioslowski, B.B. Stefanov, G. Liu, A. Liashenko, P. Piskorz, I. Komaromi, R.L. Martin, D.J. Fox, T. Keith, M.A. Al-Laham, C.Y. Peng, A. Nanayakkara, M. Challacombe, P.M.W. Gill, B. Johnson, W. Chen, M.W. Wong, C. Gonzalez, J.A. Pople, *Gaussian 03, Revision B.1*, Gaussian, Inc., Pittsburgh PA, 2003.
- [38] A.D. Becke, *J. Chem. Phys.* 98 (1993) 5648–5653.
- [39] S.H. Vosko, L. Wilk, M. Nuisar, *Can. J. Phys.* 58 (1980) 1200–1211.
- [40] C. Lee, W. Yang, R.G. Parr, *Phys. Rev. B* 37 (1988) 785–789.
- [41] B. Miehlich, A. Savin, H. Stoll, H. Preuss, *Chem. Phys. Lett.* 157 (1989) 200–206.
- [42] [a] W.J. Stevens, D.D. Konowalow, L.B. Ratcliff, *J. Chem. Phys.* 80 (1984) 1215–1224;
[b] W.J. Stevens, M. Krauss, H. Basch, P.G. Jasien, *Can. J. Chem.* 70 (1992) 612–630.
- [43] T.R. Cundari, W.J. Stevens, *J. Chem. Phys.* 98 (1993) 5555–5565.
- [44] M. Reiher, O. Salomon, B.A. Hess, *Theor. Chem. Acc.* 107 (2001) 48–55.
- [45] O. Salomon, M. Reiher, B.A. Hess, *J. Chem. Phys.* 117 (2002) 4729–4737.
- [46] [a] K. Nakamoto, *Infrared and Raman Spectra of Inorganic and Coordination Compounds: Part B, fifth edition*, Wiley, New York, 1997;
[b] W.A. Baker Jr., G.J. Long, *Chem. Commun.* (1965) 368–369.
- [47] D.A. Buckingham, F.P. Dwyer, H.A. Goodwin, A.M. Sargeson, *Aust. J. Chem.* 17 (1964) 325–336.
- [48] J.J.M. Amorre, C.J. Kepert, J.D. Cashion, B. Moubaraki, S.M. Neville, K.S. Murray, *Chem. Eur. J.* 12 (2006) 8220–8227.
- [49] [a] Z.J. Zhong, J. Tao, Z. Yu, C.-Y. Dun, Y.-J. Liu, X.-Z. You, *J. Chem. Soc. Dalton Trans.* (1998) 327–328;
[b] M. Ghazzali, V. Langer, L. Ohrstrom, *J. Solid State Chem.* 148 (1999) 350–360.
- [50] P. Metrangolo, F. Meyer, T. Pilati, G. Resnati, G. Terraneo, *Angew. Chem. Int. Ed.* 47 (2008) 6114–6127.
- [51] P. Gütllich, R. Link, A. Trautwein, In: *Mössbauer Spectroscopy and Transition Metal Chemistry*, Springer, Berlin, 1978.
- [52] K. Boukheddaden, F. Varret, *Hyperfine Interact.* 72 (1992) 349.
- [53] T. Kawamoto, S. Abe, *Chem. Commun.* (2005) 3933–3935.
- [54] I. Boldog, A.B. Gaspar, V. Martínez, P. Pardo-Ibañez, V. Ksenofontov, A. Battacharjee, P. Gütllich, J.A. Real, *Angew. Chem. Int. Ed.* 47 (2008) 6433–6437.
- [55] E. Coronado, J. Galan-Mascaros, M. Monrabal-Capilla, J. Garcia-Martinez, P. Pardo-Ibanez, *Adv. Mater.* 19 (2007) 1359–1361.
- [56] F. Volatron, L. Catala, E. Rivière, A. Gloter, O. Stéphan, T. Mallah, *Inorg. Chem.* 47 (2008) 6584–6586.
- [57] T. Forestier, S. Mornet, N. Daro, T. Nishihara, S.-I. Mouri, K. Tanaka, O. Fouché, E. Freysz, J. -F. Létard, *Chem. Commun.* (2008) 4327–4329.
- [58] J. Larionova, L. Salmon, Y. Guari, A. Tokarev, K. Molvinger, G. Molnár, A. Bousseksou, *Angew. Chem. Int. Ed.* 47 (2008) 8236–8240.
- [59] G. Molnár, S. Cobo, J.A. Real, F. Carcenac, E. Daran, C. Vieu, A. Bousseksou, *Adv. Mater.* 19 (2007) 2163–2167.
- [60] M. Cavallini, O. Bergenti, S. Milita, G. Ruani, I. Salitros, Z.-R. Qu, R. Chandrasekar, M. Ruben, *Angew. Chem. Int. Ed.* 47 (2008) 8596–8600.
- [61] M. Konno, M. Mikami-Kido, *Bull. Chem. Soc. Jpn* 64 (1991) 339–345.
- [62] J.A. Real, B. Gallois, T. Granier, F. Suez-Panama, J. Zarembowitch, *Inorg. Chem.* 31 (1992) 4972–4979.